processes

MDPI

Article

Process Integration and Optimization of the Integrated Energy System Based on Coupled and Complementary "Solar-Thermal Power-Heat Storage"

Lei Guo [1], Di Zhang [1,*], Jiahao Mi [2], Pengyu Li [2] and Guilian Liu [3]

[1] Inner Mongolia Electric Power Survery & Design Institute Co., Ltd., Hohhot 010010, China
[2] School of Energy and Power Engineering, Inner Mongolia University of Technology, Hohhot 010062, China
[3] School of Chemical Engineering and Technology, Xi'an Jiaotong University, Xi'an 710049, China
* Correspondence: zhangdi9860@126.com

Abstract: Within the context of "peak carbon and carbon neutrality", reducing carbon emissions from coal-fired power plants and increasing the proportion of renewable energy in electricity generation have become critical issues in the transition to renewable energy. Based on the principles of cascaded energy utilization, this paper improves the coupling methodology of an integrated solar thermal and coal-fired power generation system based on existing research. A parabolic trough collector field and a three-tank molten salt thermal energy storage system are connected in series and then in parallel with the outlet of the reheater. ASPEN PLUS V14 and MATLAB R2018b software were used to simulate a steady-state model and numerical model, respectively, so as to study the feasibility of the improved complementary framework in enhancing the peak load capacity of coal-fired units and reducing their carbon emissions. Actual solar radiation data from a specific location in Inner Mongolia were gathered to train a neural network predictive model. Then, the peak-shaving performance of the complementary system in matching load demands under varying hours of thermal energy storage was simulated. The findings demonstrate that, under constant boiler load conditions, optimizing the complementary system with a thermal energy storage duration of 5 h and 50 min results in an energy utilization efficiency of 88.82%, accompanied by a daily reduction in coal consumption by 36.49 tonnes. This indicates that when operated under the improved coupling framework with optimal parameters, the peak regulation capabilities of coal-fired power units can be improved and carbon emission can be reduced.

Keywords: carbon emission; coal-fired unit; three-tank molten salt heat storage system; peak regulation

check for updates

Academic Editor: Marco Vaccari

Received: 26 December 2024
Revised: 18 January 2025
Accepted: 22 January 2025
Published: 27 January 2025

Citation: Guo, L.; Zhang, D.; Mi, J.; Li, P.; Liu, G. Process Integration and Optimization of the Integrated Energy System Based on Coupled and Complementary "Solar-Thermal Power-Heat Storage". *Processes* **2025**, *13*, 356. https://doi.org/10.3390/pr13020356

Copyright: © 2025 by the authors. Licensee MDPI, Basel, Switzerland. This article is an open access article distributed under the terms and conditions of the Creative Commons Attribution (CC BY) license (https://creativecommons.org/licenses/by/4.0/).

1. Introduction

Thermal power generation remains the primary source of large-scale stable electricity supply in China and is difficult to fully replace in the short term [1]. As shown in Figure 1 in 2023 thermal power still accounts for a large proportion of the country's installed power generation capacity.By the end of 2023, China's thermal power output amounted to 6231.8 billion kilowatt-hours (kWh), constituting 69.95% of the national total power generation. Under the background of the "peak carbon and carbon neutrality" target, traditional thermal power generation technology is actively exploring improvement and transformation routes [2,3]. Among them, a photothermal-coal complementarity power generation system is a potential solution with high ecological benefits. Compared with

fossil fuel power generation technology, concentrated solar power (CSP) boasts the advantages of zero carbon emissions and no fuel costs. However, the high equipment costs associated with setting up large-scale solar collection fields and high-capacity thermal storage systems hinder the wider adoption of CSP technology [4]. Because the power generation characteristics of CSP are similar to traditional thermal power, integrating existing thermal power equipment with CSP can not only reduce the unit costs of CSP systems but also decrease the pollution emissions from thermal power units [5]. This is an effective approach to achieving energy-saving retrofits for thermal power units.

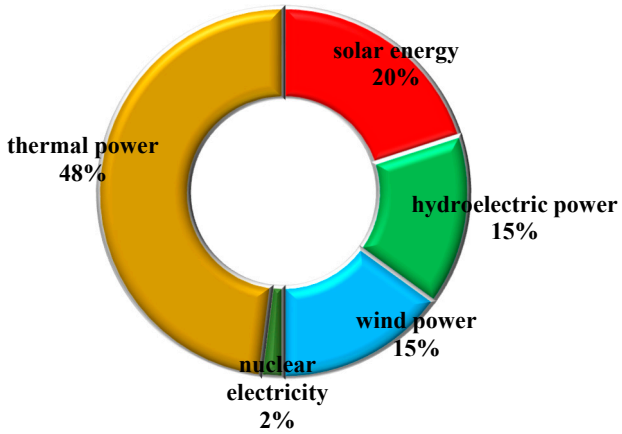

Figure 1. Proportion of the country's installed power generation capacity in 2023.

In the current research, the integration mode of thermal power units and concentrated solar power is divided into low temperature and high temperature. Low-temperature coupling was first proposed in 1975. Zoschak and Wu [6] used solar heat to replace part of the regenerative extraction steam to heat the water supply. By reducing the amount of extraction steam, the steam flow of each cylinder was increased, and the power output was improved. The thermal performance of the complementary power generation system was analyzed [7]. Since then, for complementary power generation systems, Professor Yang Yongping's [8] team at North China Electric Power University has carried out research on the coupling mechanism from both qualitative and quantitative perspectives. Hou Hongjuan et al. [9] took the 330 MW unit as the transformation object. Their research shows that the medium- and low-temperature coupling modes will affect the temperature of the main steam and the reheat steam. The coal consumption rate of the complementary system can be reduced to 258 g/kWh by using the trough collector field to replace the high-pressure heater to heat the water supply. Wu Junjie et al. [10] established a boiler variable condition model of the complementary power generation system from the perspective of total energy. The results show that the coupling point is located before the reheater, which will affect the safety of the boiler, and the thermal economy of the solar heat replacing the third stage is the best. Hui et al. [11] established a model of a complementary system without a heat storage device under the fluctuation of solar radiation. The results show that the transient disturbance of light causes a loss of up to 37.7%. Zhao Ming et al. [12] and Jiang Chengchao et al. [13] considered the influence of radiation disturbance on the actual operation of a solar-aided coal-fired complementary power generation system. Their studies concluded that the thermoelectric conversion efficiency of the medium-temperature solar heat replacing the No. 1 and No. 2 high-pressure heaters to heat the feed water reached 20.4%. During the period of high radiation, the No. 1, No. 2, and No. 3 high-pressure heaters were heated at the same time, and the thermoelectric conversion efficiency could be further improved.

High-temperature coupling involves directly heating the feed water of the coal-fired unit into high-temperature steam and sending it to the steam turbine, or preheating the exhaust steam of the unit cylinder [14], replacing part of the heat of coal combustion and reducing coal consumption. Yuan et al. [15] use high-temperature solar heat to directly heat part of the feed water into high-temperature steam and send it to the steam turbine, and its thermoelectric conversion efficiency can be increased by 0.95%. Li et al. [16] incorporated a trough solar collector field and solar industrial steam system at the exhaust end of the medium-pressure cylinder, and reheated the low-pressure cylinder inlet steam twice, which reduced the coal consumption rate under the standard working condition by 19.14 g/kWh, while the solar thermoelectric conversion efficiency was increased to 35.17%. In order to further improve the solar thermoelectric conversion efficiency of the complementary system, Yue Jiang et al. [17,18] proposed to use the tower solar energy technology with higher heat collection temperature to heat the reheat steam of the supercritical double-reheat regenerative coal-fired generating unit, so that the coal consumption rate under standard operating conditions decreased by 69.26 g/kWh, and the solar thermoelectric conversion efficiency increased to 29.1%.

However, only a simple combination of a solar collector system and a thermal power generation system will introduce the fluctuation of solar energy, which can neither reduce the influence of light disturbance nor ensure the continuous supply of solar heat to the complementary system. If the coal-fired power generation system is less coupled with light heat, it cannot effectively reduce the carbon emissions of the unit. Li Bin et al. [19] sent the feed water from the outlet of the high-pressure heater into the tower solar boiler to heat the high-temperature steam and sent it to the high-pressure cylinder to perform work. The dynamic simulation results of real-time simulation prove that solar energy makes the boiler start and stop frequently due to intermittence, which will aggravate the life loss of low cycle fatigue.

Therefore, scholars have combined the heat storage system with the solar-assisted coal-fired power generation system to maximize the advantages of thermal power generation and solar thermal power generation. Yong Zhu et al. [20] simulated the tower solar collector system in series with the reheater of a 1000 MW coal-fired unit and collected solar energy heat through a double-tank molten salt heat storage system so that the complementary power generation system can use solar energy to generate 214.7 MW. Hongtao Liu et al. [21] paralleled the heat collection system with the regenerative cycle of coal-fired units and established a solar energy prediction model, which verified that the parallel mode and pre-scheduling were beneficial to improve the stability of the system. Lei et al. [22] simulated five complementary power generation coupling methods of tower solar heating main steam, reheat steam, secondary heating steam, heating water supply, flue gas, and high-temperature steam heat recovery. Through comparison, it is proved that the tower collector system is connected in parallel with the regenerative cycle, and the energy-saving efficiency of the complementary system is the highest. Zhang et al. [23,24] demonstrated the feasibility of collecting high-temperature flue gas and superheated steam in coal-fired power plants for deep peak shaving and proposed the use of a molten salt heat storage system to store reheat steam heat to improve the peak-shaving performance of the unit. The results show that the latent heat storage method has a larger energy density and better peak-shaving effect than the sensible heat storage method.

At present, extensive research has been conducted on the utilization of heat storage systems for storing low-temperature or high-temperature solar thermally coupled regenerative cycles to enhance unit peak load power supply capacity and mitigate carbon emissions. However, limited attention has been given to investigating the application of heat storage

systems in enhancing unit peak regulation flexibility and optimizing system configuration and operational parameters.

Due to the different time scales and uncertainties of the thermal load, electrical power output, and solar radiation intensity in the complementary power generation system [25,26] and the fluctuating nature of short-term power load, it is necessary to establish corresponding prediction models to reduce the instability introduced by the integration of solar energy into the complementary system, to avoid waste of heat and electricity in the complementary system under load fluctuations, and to reduce energy waste. The back propagation (BP) neural network is one of the most widely used neural network models with high maturity and is also a local search optimization method, prone to falling into local optima; it has a slow convergence speed when dealing with large-scale data or complex models. In response to its shortcomings, researchers have improved its performance and effectiveness through neural network parameter optimization [27,28] and neural network structure adjustment [29,30].

Under the trend of large-scale grid integration of renewable energy, thermal power units are facing new operating conditions such as deep and frequent peak shaving. It is necessary to establish a complementary power generation model with a better economy, peak-shaving performance and coal-saving effect. Therefore, based on the principle of temperature matching and energy cascade utilization, this paper uses the three-tank molten salt system to combine the heat storage and peak-shaving process of the unit and the solar heat collection process and uses the system energy in stages to construct an improved 'solar-thermal power-heat storage' coupling and complementary power generation process. Considering both the cost of conventional peak regulation and unit transformation into a complementary system, the parameter configuration of the complementary system is optimized, and the optimal heat storage time operation parameters of the complementary system under known load and radiation data are obtained with the maximum energy utilization efficiency as the optimization target. The reliability of the power load prescheduling of the complementary power generation system is improved, and the transition of thermal power generation from the power supply of the power grid to the regulating power supply is realized.

2. "Solar-Thermal Power-Heat Storage" Integrated Power Generation System

Improved coupling diagram of complementary power generation system is shown in Figure 2. When the light intensity is high during the day, the complementary system collects solar radiation heat energy through the trough collector field. It heats the low-temperature molten salt C_{out} and transfers it to the medium-temperature tank for storage. When the grid-side load demand exceeds the coal-fired unit's electric load output, valve V2 opens to introduce deoxygenated water f_0. The medium-temperature molten salt and high-temperature molten salt are directed to heat exchangers EX3 and EX1, respectively. The f_0 is gradually heated to superheated steam S_f, which powers the medium-pressure cylinder, thereby enhancing the electric energy output of the complementary power generation system.

2.1. System Modelingcoal-Fired Unit

2.1.1. Process Simulation

In this paper, a subcritical 600 MW coal-fired power unit is investigated as the subject of analysis. To ascertain the reliability of the ASPEN PLUS V14 model, the comparison between design parameters and simulation results under typical operating conditions at 50% Turbine Heat Acceptance (THA) is presented in Table 1.

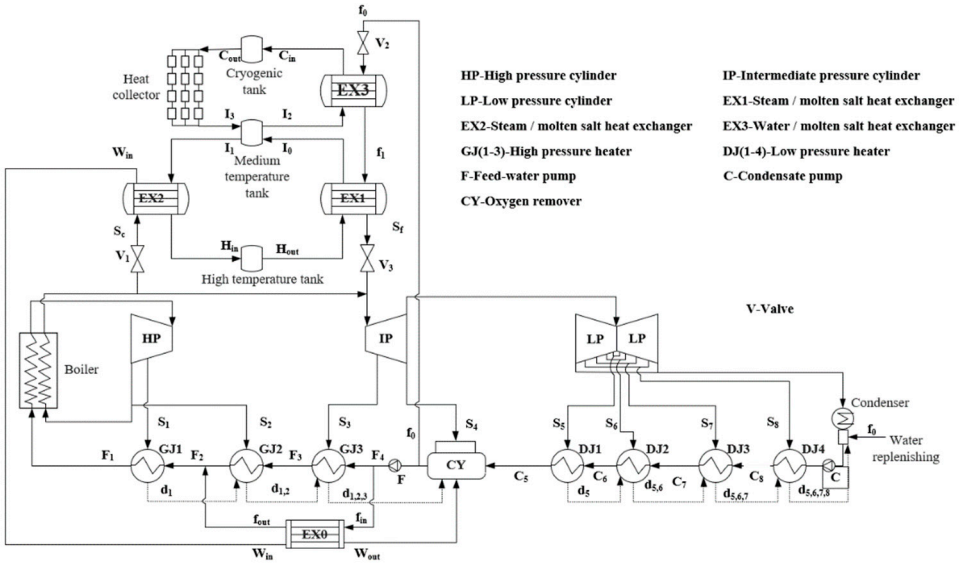

Figure 2. Improved coupling diagram of complementary power generation system (Based on the principle of energy cascade utilization, this paper integrates steam extraction and heat storage with solar heat collection through a three-tank heat storage system: when the power grid's load demand is less than the electric load output of the coal-fired unit, excess reheat steam is extracted from the valve V1 and sent to the heat exchanger EX2. It undergoes a phase change into water W_{in}. Then, W_{in} enters the heat exchanger EX0 to heat the boiler feed water of the regenerative cycle and recover the waste heat. The molten salt stream I_1 of the medium-temperature tank absorbs the phase change heat of steam in the heat exchanger EX2, heating it into high-temperature molten salt $H_{in.}$ Subsequently, the heated molten salt is directed into the high-temperature tank for storage. The steam extraction and heat storage process reduces the amount of steam that performs work in the intermediate pressure turbine, thereby decreasing power generation.).

Table 1. Comparison of 50%THA design parameters and simulation parameters.

Parameter Name	Unit	Design Parameter	Modeling Results	Error
output power	kW	300,080	295,540	1.5%
main steam flow	kg/h	938,620	938,620	0%
main steam temperature	°C	538	538	0%
reheat steam flow	kg/h	826,332	826,332	0%
reheated steam temperature	°C	520	520	0%
condensed water temperature	°C	32.54	33.52	3.1%
feed water temperature	°C	238.9	238.7	0.05%
the first-stage extraction steam temperature	°C	370.6	365.31	1.4%
the second-stage extraction steam temperature	°C	314.1	310.7	1.08%
the third-stage extraction steam temperature	°C	439.9	439.64	0.06%
GJ1 Feedwater/drainage temperature	°C	238.9/219.1	238.7/219.8	0.05%/0.3%
GJ2 Feedwater/drainage temperature	°C	213.5/187.7	214.2/185.3	0.3%/1.3%
GJ3 Feedwater/drainage temperature	°C	182.1/174	179.7/173.4	1.3%/0.3%

2.1.2. Numerical Simulation

The complementary power generation system adjusts the power generation of the unit by varying the steam mass flow rate at the reheater outlet. After the reheater, the units at all levels are in a state of variable operating conditions. When the steam flow rate changes, the extraction steam temperature at all levels is calculated by using the Formula (1) Frügel formula [25].

$$\frac{D_1}{D_{10}} = \frac{\sqrt{P_1^2 - P_2^2}}{\sqrt{P_{10}^2 - P_{20}^2}} \frac{\sqrt{T_{10}}}{\sqrt{T_1}} \quad (1)$$

where D_{10} and D_1 are the steam mass flow rate before and after the variable condition, kg/h; P_{10} and P_{20} are the pressure of the front and rear stages of the stage group before the variable operation condition, MPa; P_1 and P_2 are the pre-stage and post-stage pressures of the stage after the variable operation condition, MPa; T_{10} and T_1 are the steam temperature before and after the variable operation condition, °C.

After the change in steam extraction amount, the relationship between steam, feed water, and step-by-step self-flow drainage in the surface regenerative heater can be mathematically described by Formulas (2)–(4) [31].

$$q_i = h_{s,i} - h_{d,i} \tag{2}$$

$$\gamma_i = h_{d,i} - h_{d,i+1} \tag{3}$$

$$\tau_i = h_{w,i} - h_{w,i+1} \tag{4}$$

where q_i, γ_i, and τ_i are the specific enthalpy difference of steam heat release, the specific enthalpy difference of drainage heat release, and the specific enthalpy rise of feed water heat absorption, kJ/kg; $h_{s,i}$ is the specific enthalpy of extraction, kJ/kg; $h_{d,i}$ and $h_{d,i+1}$ are the specific enthalpy values of the upper and lower levels, kJ/kg. $h_{w,i}$ and $h_{w,i+1}$ are the specific enthalpy values of the outlet feed water and the inlet feed water, kJ/kg.

Without considering shaft seal leakage and heat loss of heaters and pipes, the ideal heat balance equation of steam-water cycle can be expressed as Formula (5) by using the matrix method [26,27,32].

$$\begin{bmatrix} q_1 & & & & & & & \\ \gamma_1 & q_2 & & & & & & \\ \gamma_2 & \gamma_2 & q_3 & & & & & \\ \gamma_3 & \gamma_3 & \gamma_3 & q_4 & & & & \\ & & & & q_5 & & & \\ & & & & \gamma_5 & q_6 & & \\ & & & & \gamma_6 & \gamma_6 & q_7 & \\ & & & & \gamma_7 & \gamma_7 & \gamma_7 & q_8 \end{bmatrix} \cdot \begin{bmatrix} D_1 \\ D_2 \\ D_3 \\ D_4 \\ D_5 \\ D_6 \\ D_7 \\ D_8 \end{bmatrix} = \begin{bmatrix} D_{fw}\tau_1 \\ (D_{fw} + \Delta D_f)\tau_2 \\ (D_{fw} + \Delta D_f)\tau_3 \\ D_{fw}\tau_4 \\ D_{cw}\tau_5 \\ D_{cw}\tau_6 \\ D_{cw}\tau_7 \\ D_{cw}\tau_8 \end{bmatrix} \tag{5}$$

where D_i, D_{fw}, D_{cw}, and ΔD_f are the mass flow rate of extraction steam, the mass flow rate of feed water, the flow rate of condensate water, and the variation in feed water in the regenerative cycle, kg/h.

Based on the minimum technical output, conventional coal-fired power units achieve deep peak shaving by reducing unit performance or resorting to oil-assisted combustion at low boiler loads. The peak-shaving section of the thermal power unit is illustrated in Figure 3.

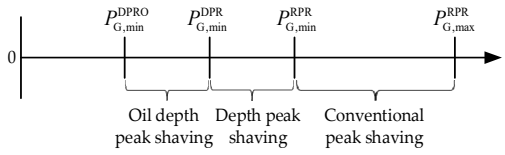

Figure 3. Schematic diagram of peak load zone of thermal power unit.

Here, P_G is the unit output, kW; the superscripts RPR, DPR, and DPRO are the normal operation of the unit, the deep peak regulation without oil injection, and the deep peak regulation with oil injection, respectively. The values correspond to 60%, 45%, and 30% of

the unit's maximum output capacity. The subscripts min and max are the minimum and maximum values.

$$\begin{cases} k_{G,t}^{RPR} \cdot P_{G,min}^{RPR} \le P_{G,t} \le k_{G,t}^{RPR} \cdot P_{G,max}^{RPR} \\ k_{G,t}^{DPR} \cdot P_{G,min}^{DPR} \le P_{G,t} \le k_{G,t}^{DPR} \cdot P_{G,max}^{DPR} \\ k_{G,t}^{DPRO} \cdot P_{G,min}^{DPRO} \le P_{G,t} \le k_{G,t}^{DPRO} \cdot P_{G,max}^{DPRO} \end{cases} \quad (6)$$

where k is used to limit the operating state of the unit, with a value of only 0 or 1, and the constraint is

$$k_{G,t}^{RPR} + k_{G,t}^{DPR} + k_{G,t}^{DPRO} = 1 \quad (7)$$

The output constraint of the storage and release process of the complementary system is

$$P_{R,t} = P_{G,t} - k_{char,t} \cdot P_{char,t} + k_{dis,t} \cdot P_{dis,t} \quad (8)$$

where $P_{R,t}$ is the output of the complementary system, MW; $P_{char,t}$ and $P_{dis,t}$ are the stored and increased power output of the complementary system, MW. Here, k_{char} and $k_{dis,t}$ are heat storage and heat release instructions, and their values are only 0 or 1. This paper assumes that heat storage and heat release cannot be carried out simultaneously.

$$k_{char,t} \cdot k_{dis,t} = 0 \quad (9)$$

2.2. Ideal Model of Heat Storage and Release Process

2.2.1. Subsystem Ideal Thermal Power Calculation

The balance between heat storage and release power is solely evaluated based on the total energy in this study. When storing heat, the power for heating molten salt by high-temperature reheated steam and the power of heating feedwater by hot saturated water can be mathematically expressed as [33,34]

$$Q_{char1} = \eta_{ex} D_{sc}(h_{sc} - h_{win}) = D_{I1} C_p (T_{hin} - T_{I1}) \quad (10)$$

$$Q_{char2} = \eta_{ex} D_{sc}(h_{win} - h_{wout}) = D_{fin}(h_{fout} - h_{fin}) \quad (11)$$

where η_{ex} is the heat exchanger efficiency, taken to be 98%; D_{sc}, D_{I1}, and D_{fin} are the steam extraction flow for thermal storage, medium-temperature molten salt mass flow, and bypass feed water flow, kg/h. h_{sc}, h_{win}, and h_{wout} are the specific enthalpy values of the reheat steam, saturated water inlet, and saturated water outlet, kJ/kg; T_{hin} and T_{I1} are high-temperature and medium-temperature molten salt temperature, °C; h_{fout} and h_{fin} are the specific enthalpies of the bypass feedwater outlet and inlet, kJ/kg.

When releasing heat, the power for heating steam with high-temperature molten salt and the power of heating feedwater with stored solar heat can be mathematically expressed as [33,34]

$$Q_{dis1} = \eta_{ex} D_{hout} C_p (T_{hout} - T_{I0}) = D_{f0}(h_{sf} - h_{f0}) \quad (12)$$

$$Q_{dis2} = \eta_{ex} D_{I2} C_p (T_{I2} - T_{Cin}) = D_{f0}(h_{f1} - h_{f0}) \quad (13)$$

where D_{hout}, D_{I1}, and D_{f0} are the mass flow rate of high-temperature and medium-temperature molten salt and the bypass water flow rate, kg/h; h_{sf} and h_{f1} are the inlet enthalpy of reheat steam and saturated water, kJ/kg. T_{hout}, T_{I0}, and T_{Cin} are high-temperature, medium-temperature, and low-temperature molten salt temperature, °C; h_{f1} and h_{f0} are the specific enthalpy of the bypass feedwater outlet and inlet, kJ/kg.

2.2.2. Heat Storage System

Assuming the storage tank adopts an ideal thermodynamic model [35,36], the mass and energy conservation of heat storage and release can be expressed as Equations (14) and (15).

$$q_{m,in} - q_{m,out} = \frac{dM}{dt} \tag{14}$$

$$q_{m,in} C_{p,in} T_{in} - q_{m,out} C_p T - Q_{\text{loss}} = \frac{dMC_pT}{dt} \tag{15}$$

where $q_{m,in}$ and $q_{m,out}$ are the molten salt flow into and out of the tank, kg/s; M is the mass of molten salt in the tank, kg; t is the running time of the heat storage system, s; $C_{p,in}$ and C_p are the specific heat capacity of molten salt flowing into and out of the tank, J/kg·K^{-1}; T_{in} and T are the molten salt temperature that flows into and out of the tank, K.

The molten salt is fully mixed, the temperature is evenly distributed, and the heat loss Q_{loss} is expressed in Formula (16) [33,34,37].

$$\begin{aligned} Q_{\text{loss}} &= \chi \cdot Q_{\text{loss,full}} + (1-\chi) \cdot Q_{\text{loss,empty}} \\ \chi &= (M - M_{\text{min}}) / (M_{\text{max}} - M_{\text{min}}) \end{aligned} \tag{16}$$

where λ is the storage of molten salt in the tank; $Q_{\text{loss,full}}$ and $Q_{\text{loss,empty}}$ are the average heat loss rate of the maximum and minimum amount of molten salt stored in the storage tank, W; M_{min} and M_{max} are the minimum and maximum reserves of the heat storage tank, kg.

2.2.3. Direct Radiation Short-Term Prediction Model

The time scales of heat load, electric power output, and solar radiation in the complementary system exhibit variability and uncertainty. In this paper, the BP neural network time series prediction model is used to estimate the short-term radiation data and the solar thermal pre-scheduling. BP neural network training mainly covers two stages: forward propagation and back propagation:

(1) Forward propagation: The dataset is input into the hidden layer feedforward transfer function, and the output signal is generated by nonlinear transformation. The error is calculated by comparison with the actual value. If the error exceeds the preset threshold, the back propagation is started.

(2) Back propagation: The error obtained by forward propagation is transmitted layer by layer from the output layer to the input layer through the hidden layer and distributed to each unit. According to the error signals of each layer, the connection weights and thresholds of input-hidden layer and hidden layer-output layer nodes are adjusted to make the error decrease along the gradient. After several iterations of training, the network weights and thresholds corresponding to the minimum error are determined.

Training effect of direct solar radiation prediction model is shown in Figure 4.

Correlation values (R-values) are usually calculated using the Pearson correlation coefficient, as follows [38]:

$$R = \frac{\sum_{\text{i=1}}^{\text{n}} (x_i - \overline{x})(y_i - \overline{y})}{\sqrt{\sum_{\text{i=1}}^{\text{n}} (x_i - \overline{x})^2 \sum_{\text{i=1}}^{\text{n}} (y_i - \overline{y})^2}} \tag{17}$$

where n is the number of samples; x_i is the actual value of the first sample; $\overline{x}$ is the average of the actual values; y_i is the predicted value of the first sample; $\overline{y}$ is the average of the predicted values.

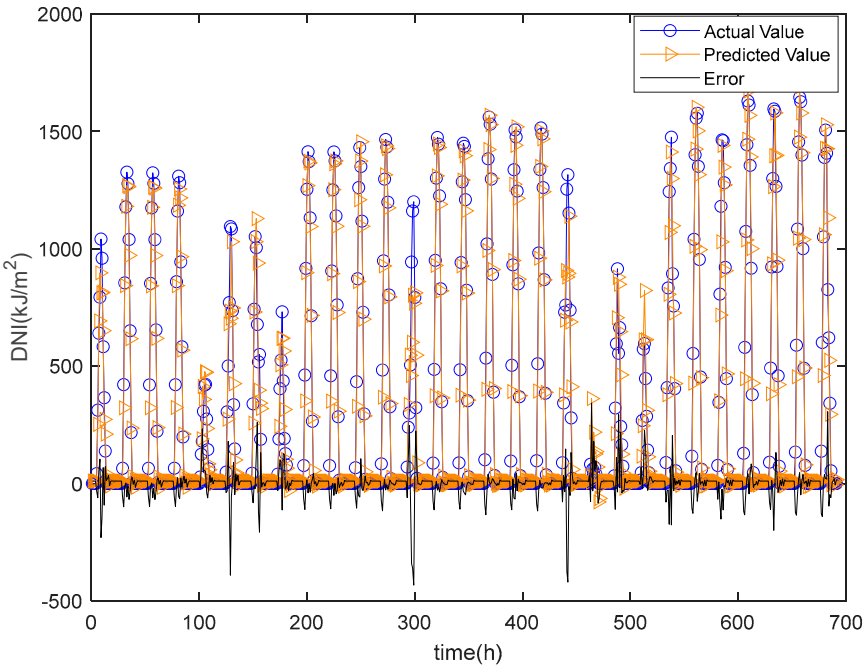

Figure 4. Training effect of direct solar radiation prediction model.

The distribution of model training error is shown in Figure 5. The R-value is usually between −1 and 1. Usually, when its absolute value is greater than 0.8, it means that the predicted value after training is correlated with the actual value, which can be used for engineering prediction. Based on the R-value analysis, it is evident that the model yields more accurate prediction results.

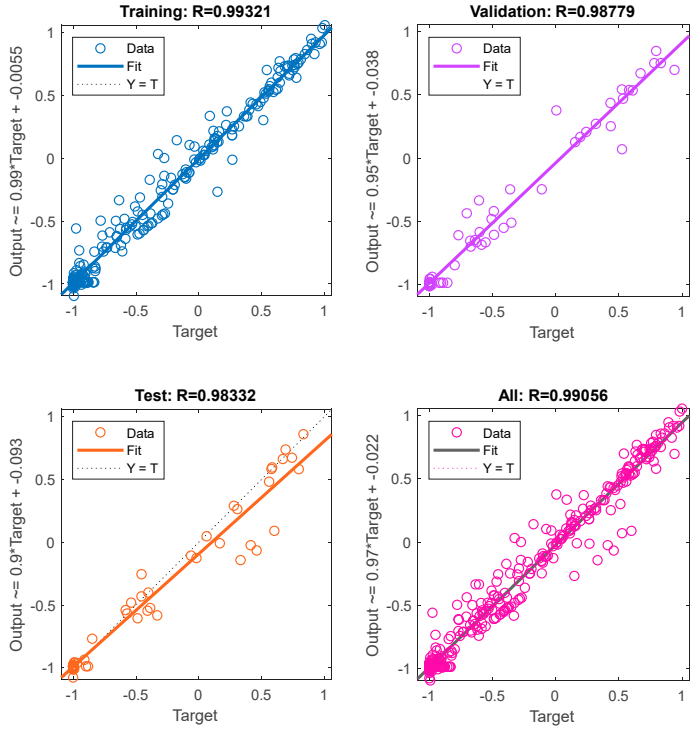

Figure 5. DNI predicts training R-value distribution.

The short-term direct solar radiation is predicted and compared with the actual value, as shown in Figure 6.

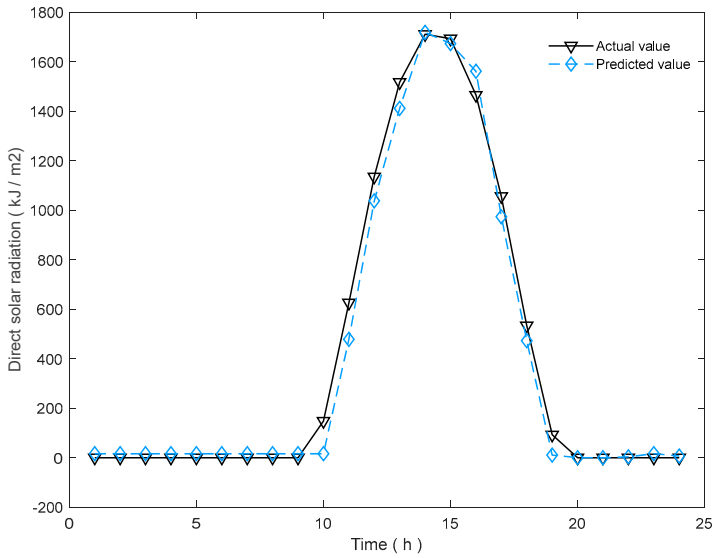

Figure 6. Comparison of DNI prediction results with actual values.

3. Integration and Optimization of Complementary System

3.1. Economic Load of Unit Peak Load Regulation Operation

Based on the lowest point of boiler fuel consumption and unit life cost, the benchmark output of peak-shaving operation in this paper is determined.

$$C_{G,R} = C_{G,MC} + C_{G,fuel} \tag{18}$$

where $C_{G,fuel}$ is the boiler fuel cost; $C_{G,MC}$ is the rotor life loss cost.

During the conventional peak-shaving operation of the unit, rapid alteration of steam flow subjects the rotor to significant alternating thermal stresses, resulting in fatigue-induced wear over repeated cycles. The simplified Manson-Coffin formula [39] is used to describe the impact of the peak-shaving output on the life cost of the rotor:

$$C_{G,MC} = \sum_{t=1}^{T}\left[\frac{C_G}{2N_{F,G,t}} \cdot (\beta_1 \cdot k_{G,t}^{DPR} + \beta_2 \cdot k_{G,t}^{DPRO} + \beta_3 \cdot k_{G,t}^{RPR})\right] \tag{19}$$

where T is the operating duration of the unit, h; C_G is the cost of purchasing the unit, with the price of 4458 CNY/kWh; the loss coefficients of β_1, β_2, and β_3 are 1.3, 1.4, and 1.2 respectively for no oil, oil, and normal operation. $N_{F,G,t}$ is the t-hour rotor cracking cycle of the unit, which is closely related to the output power of the unit. The empirical formula summarized by the predecessors is as follows [40]:

$$N_{F,G,t} = 0.005778(P_{G,t})^3 - 2.682(P_{G,t})^2 + 484.8P_{G,t} - 8411 \tag{20}$$

The stability of combustion and hydrodynamics in the boiler is compromised during low-load operation. In this paper, the cost of additional coal combustion and combustion-supporting oil is considered.

$$C_{G,fuel} = C_{G,oil} + C_{G,coal} = \sum_{t=1}^{T} c_{oil,t} \cdot S_{oil} + \sum_{t=1}^{T} b_{cp,t} \cdot P_{G,t} \cdot S_{coal} \tag{21}$$

where $C_{G,oil}$ is the oil input cost of low-load stable combustion of the boiler, and the oil price S_{oil} is 6130 CNY/t; $c_{oil,t}$ is the amount of oil input for stable combustion at low load

during t period of the boiler, t; $b_{cp,t}$ is the coal consumption rate of the whole plant at time T, g/kWh; standard coal price S_{coal} is 800 CNY/t.

The substitution of the unit operating condition data into the Formula (17) simulation is shown in Figure 7.

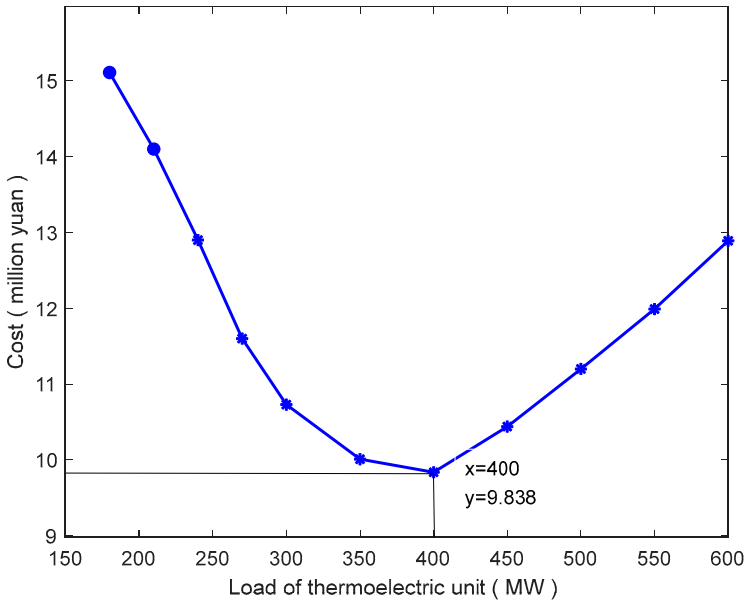

Figure 7. Changes in conventional unit costs.

The results show that the unit load value is adjusted to the lowest cost of 400 MW, so the subsequent peak-shaving operation of the unit is based on the 400 MW benchmark, and the system power output is adjusted by varying the thermal load of the heat storage system.

The results indicate that the lowest cost is achieved when the unit load value is adjusted to 400 MW. Therefore, the subsequent peak load operation of the unit will be based on a benchmark of 400 MW, and the system's electrical energy output will be adjusted by regulating the thermal load of the heat storage system.

3.2. Configuration Optimization of Heat Storage and Heat Collection System

The load regulation of the heat storage system is influenced by factors such as the heat exchanger, molten salt quality, and heat collection area. This paper assumes that the adjustment of the heat exchanger per unit time does not exceed 15% THA, and it converts the heat collection area and the quality of the molten salt per unit price and the peaking power into cost [17,18]. The minimum value of Formula (23) is used as the configuration of the molten salt quality and the heat collection area of the complementary system:

$$LCOE = \frac{\left(\frac{k_{debt}\cdot(1+k_{debt})^N}{(1+k_{debt})^N-1} + k_{ins}\right)\cdot C_{inv} + C_{O\&M}}{E_{re}} \quad (22)$$

where $LCOE$ is the peaking power cost of system transformation, CNY/kWh; k_{debt} is debt interest, 8%; N is the complementary system lifetime, 20 years; k_{ins} is the insurance interest, 1%; C_{inv} is the average daily cost of heat storage and heat collection systems; $C_{O\&M}$ is the operation and maintenance cost of the system; E_{re} is peaking power, kWh.

The simulation results of Formula (22) are shown in Figure 8. The red dot indicates the minimum LCOE value, determined to be 1.15 CNY/kWh, corresponding to a molten salt mass of 1.7×10^4 t and a heat collection area of 5.027×10^4 m^2.

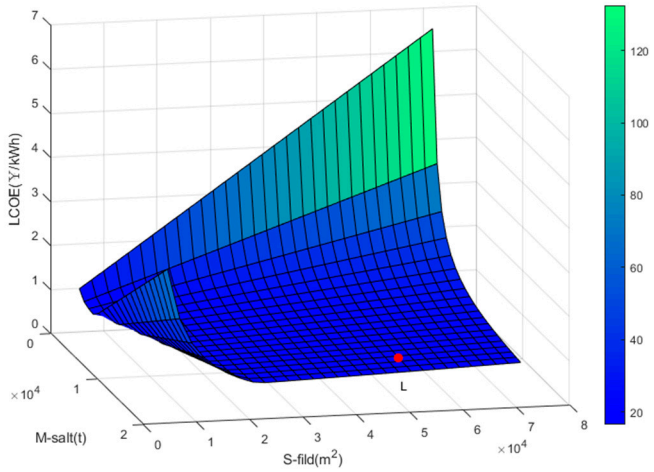

Figure 8. Effect of molten salt and heat collecting area change on the cost of homogenized power.

3.3. Optimization Object

The load data of a power plant are shown in Figure 9, and the solar radiation data are shown in Figure 6.

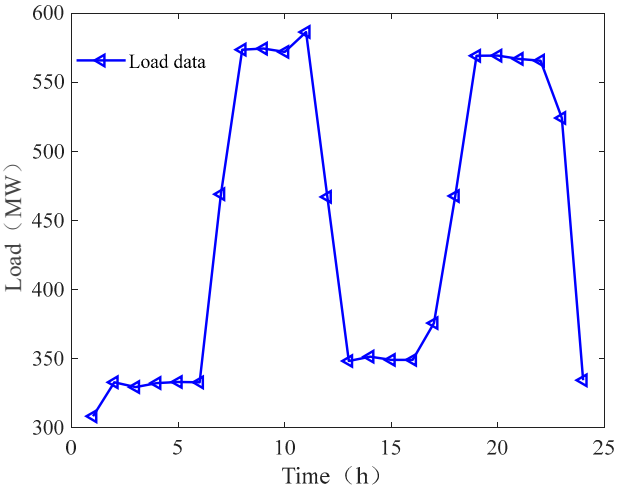

Figure 9. Daily load demand data.

The amount of coal saved is converted by the solar energy used in the heat release process of the system:

$$B_{\text{save}} = \frac{\int_0^{t_{\text{dis}}} D_{\text{f0}}(h_{\text{f1}} - h_{\text{f0}})dt}{q_{\text{coal}}} \tag{23}$$

where B_{save} is the amount of coal saved by the complementary system, t.

There is a deviation between the ideal load regulation output of the complementary system and the actual load. The ratio of the sum of the difference between the output of each period and the actual load to the sum of the actual load is the energy utilization efficiency of the complementary system with T-hour heat storage operation:

$$\eta_T = (1 - \frac{\left|\sum_{t=1}^{24}(P_{\text{load},t} - P_{\text{R},t} - Q_{\text{loss}})\right|}{\sum_{t=1}^{24} P_{\text{load},t}}) \cdot 100\% \tag{24}$$

where η_T is the energy utilization rate adjusted by T-hour heat storage, %; $P_{\text{load},t}$ is the load demand value at time t, MW.

3.4. Optimization Step

(1) According to the Formula (17) simulation, the boiler output is optimized at 400 MW, resulting in the minimal cost of coal consumption and operational life.

(2) The heat exchanger is configured to accommodate a maximum adjustment of 90 MW of load per unit time, with the molten salt mass and heat collection area serving as variables, and the lowest point of the Formula (23) simulation is configured as the initial value.

(3) The heat is initially stored and subsequently released by the system. The load parameters are calculated using Formulas (6)–(9), and the ASPEN PLUS V14 model is adjusted to simulate variations in reheat steam.

(4) The heat storage and release time is set to be the same, and the heat release process is uniform. Steam extraction parameters under varying operational conditions are calculated by Formulas (1)–(5), while the subsystem mass and energy conservation are determined through calculations based on Formulas (10)–(16).

(5) The thermal parameters of the system are calculated by Formulas (23) and (24). The specific process is shown in Figure 10.

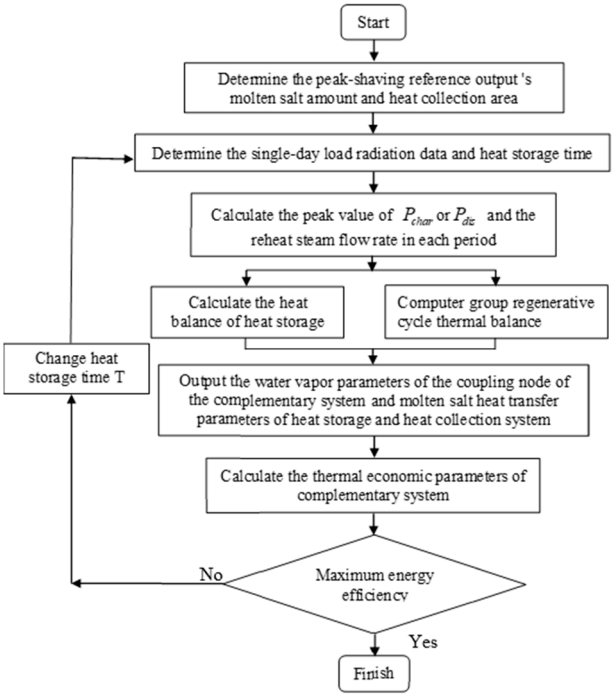

Figure 10. "Solar-thermal-storage" complementary power generation system calculation flow.

4. Results and Discussion

The initial heat storage time is set at 4 h, with an adjustment range of 4 to 8 h, and the load data undergo an initial change step of 1 h. The preliminary adjustment results are included in Table 2.

Table 2. Heat storage for 4 to 8 h of system operation results.

Evaluation Index	Unit	4	5	6	7	8
Net coal saving amount	t/d	45.96	34.09	36.58	33.62	29.97
variability energy	%	71.76	80.59	88.43	80.92	74.84

The data presented in Table 2 indicate that the optimal heat storage time for achieving the maximum energy utilization efficiency of the system is approximately 6 h. The heat

storage time is adjusted for 20 min before and after the change. The results are included in Table 3, and the curve of energy utilization efficiency with heat storage time is drawn as shown in Figure 11.

Table 3. Heat storage for 5 h 40 min to 6 h 20 min as a result of system operation.

Evaluation Index	Unit	5 h 40 min	5 h 50 min	6 h 10 min	6 h 20 min
Net coal saving amount	t/d	35.53	36.49	35.41	34.99
variability energy	%	88.42	88.82	86.84	85.89

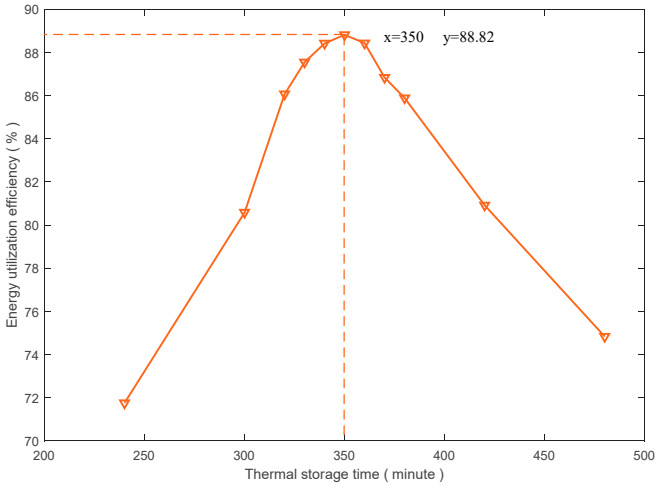

Figure 11. Effect of heat storage time on parameters.

The results in Figure 11 demonstrate that the energy utilization efficiency of the complementary system initially increases and then decreases with an increase in heat storage time. Notably, when the heat storage time reaches 5 h and 50 min, the system achieves its maximum energy utilization efficiency. The load regulation performance of the complementary system is illustrated in Figure 12. Due to a fluctuation period of approximately 6 h, there are two peaks and valleys within a day. When the heat storage time is less than 6 h, frequent power regulation processes lead to power wastage. Conversely, when the heat storage time exceeds 6 h, it becomes challenging to promptly respond to load demands and effectively utilize stored high-temperature heat energy for waste heat generation.

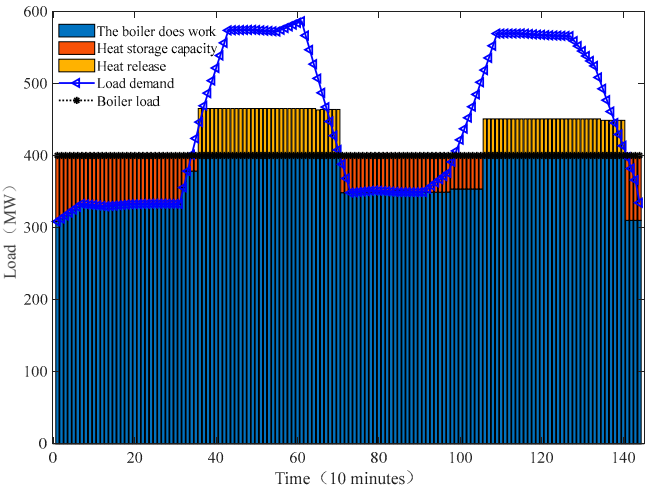

Figure 12. Result of system storing heat for 5 h 50 min.

This paper combines the peak-shaving process of the unit and the solar coupled thermal cycle process based on the principle of energy cascade utilization, and the three-tank heat storage system is employed to simultaneously store excess high-temperature steam heat energy during the valley power period of the unit. The varying operation condition process model is simulated in ASPEN PLUS V14, and the influence of reheat steam change on the water vapor parameters and power output of the unit is obtained. Additionally, a numerical model in MATLAB R2018b is developed to verify and calculate subsystem parameter changes under variable working conditions. When the boiler output load is fixed, given short-term load and solar radiation fluctuations, the reheater steam flow is adjusted through the energy storage system to match demand requirements. The results demonstrate the following:

(1) After the coupling transformation of the complementary system, the closer the heat storage and release time in a single day is to the load change rule, the greater the heat energy utilization efficiency is.
(2) Based on simulation results, adjusting heat storage time by 5 h and 50 min yields optimal energy utilization efficiency for this paper's load.
(3) Because the solar heat used by the c system is related to the heat release process, the longer the heat storage time, the shorter the single-day heat release operation time, and the less the solar energy saving.

In this study, the parameter configuration of the complementary system is optimized; taking the maximum energy utilization efficiency as the optimization objective, the optimal heat storage time operation parameters of the complementary system under the known load and radiation data are obtained, which provides a certain theoretical basis for the flexible transformation of thermal power plants. This has important practical guiding significance for thermal power plants to reduce the transformation cost, improve the operation efficiency, and promote the efficient and orderly development of the flexibility transformation work. It is expected to provide strong support for the technological upgrading and sustainable development of the thermal power industry.

Author Contributions: Methodology, D.Z.; Formal analysis, L.G. and G.L.; Data curation, J.M. and P.L. All authors have read and agreed to the published version of the manuscript.

Funding: This work was supported by the Inner Mongolia Science and Technology Plan Project (2023YFHH0108) and Postdoctoral Research Project (41510023012).

Data Availability Statement: The original contributions presented in the study are included in the article; further inquiries can be directed to the corresponding author.

Acknowledgments: Special thanks are given to the editor and the anonymous reviewers for their valuable advice and comments on the manuscript.

Conflicts of Interest: Authors Lei Guo and Di Zhang were employed by the company Inner Mongolia Electric Power Survery & Design Institute Co., Ltd. The remaining authors declare that the research was conducted in the absence of any commercial or financial relationships that could be construed as a potential conflict of interest.

References

1. Wu, J.; Hou, H.; Hu, E.; Yang, Y. Performance improvement of coal-fired power generation system integrating solar to preheat feedwater and reheated steam. *Sol. Energy* **2018**, *163*, 461–470. [CrossRef]
2. Wang, D.; Liu, D.; Wang, C.; Zhou, Y.; Li, X.; Yang, M. Flexibility improvement method of coal-fired thermal power plant based on the multi-scale utilization of steam turbine energy storage. *Energy* **2022**, *239*, 122301. [CrossRef]
3. Wang, C.; Zhao, Y.; Liu, M.; Qiao, Y.; Chong, D.; Yan, J. Peak shaving operational optimization of supercritical coal-fired power plants by revising control strategy for water-fuel ratio. *Appl. Energy* **2018**, *216*, 212–223. [CrossRef]

4. Gonzalez-Salazar, M.A.; Kirsten, T.; Prchlik, L. Review of the operational flexibility and emissions of gas-and coal-fired power plants in a future with growing renewables. *Renew. Sustain. Energy Rev.* **2018**, *82*, 1497–1513. [CrossRef]
5. Sun, Y.; Xu, C.; Xin, T.; Xu, G.; Yang, Y. A comprehensive analysis of a thermal energy storage concept based on low-rank coal pre-drying for reducing the minimum load of coal-fired power plants. *Appl. Therm. Eng.* **2019**, *156*, 77–90. [CrossRef]
6. Lei, F. Optimization Design and Thermal Performance Analysis of Solar-Coal Hybrid Power Generation System. Ph.D. Thesis, North China Electric Power University, Beijing, China, 2016.
7. Pang, L.; Zhang, S.; Duan, L. Research on improving the flexibility of double reheat unit by high temperature molten salt energy storage. *Chin. J. Electr. Eng.* **2021**, *41*, 2682–2691.
8. Li, X.; Wei, H.; Liu, M.; Zhao, Y.; Wang, Z.; Yan, J. Simulation study on dynamic characteristics of 660 MW solar-coal complementary system. *Chin. J. Eng. Thermophys.* **2020**, *41*, 1837–1844.
9. Hou, H.; Wang, X.; Song, H.; Cui, H.; Yue, R.; Zhao, J. Analysis of dynamic characteristics and annual performance of solar-assisted 330 MW coal-fired unit complementary power generation system. *Acta Energ. Solaris Sin.* **2018**, *39*, 3331–3338.
10. Wu, J.; Han, Y.; Sun, Y. Study on the off-design performance of solar-coal complementary power generation system. *Acta Energ. Solaris Sin.* **2022**, *43*, 345–350.
11. Yan, H.; Liu, M.; Chong, D.; Wang, C.; Yan, J. Dynamic performance and control strategy comparison of a solar-aided coal-fired power plant based on energy and exergy analyses. *Energy* **2021**, *236*, 121515. [CrossRef]
12. Zhao, M.; Chen, X.; Liang, J.; Liu, Y. Research on the performance of solar-coal hybrid power generation system under compound disturbance conditions. *Acta Energ. Solaris Sin.* **2018**, *39*, 2252–2259.
13. Jiang, C.; Wang, P.; Hao, Y.; Zhao, M.; Li, M.; Liang, J. Research on integration scheme and performance analysis of solar-coal complementary power generation system. *J. Sol. Energy* **2018**, *39*, 988–995.
14. Shagdar, E.; Shuai, Y.; Lougou, B.G.; Mustafa, A.; Choidorj, D.; Tan, H. New integration mechanism of solar energy into 300 MW coal-fired power plant: Performance and techno-economic analysis. *Energy* **2022**, *238*, 122005. [CrossRef]
15. Wang, Y.; Liu, J.; Zhang, C.; Hu, S.; Zhang, Y. Heat storage design and performance analysis of a parabolic trough thermal power generation system based on sectional heating collection. *J. Energy Storage* **2022**, *51*, 104572. [CrossRef]
16. Li, J.; Xin, Y.; Hu, B.; Zeng, K.; Wu, Z.; Fan, S.; Li, Y.; Chen, Y.; Wang, S.; Wang, J.; et al. Safety and thermal efficiency performance assessment of solar aided coal-fired power plant based on turbine steam double reheat. *Energy* **2021**, *226*, 120277. [CrossRef]
17. Jiang, Y.; Duan, L.; Yang, M.; Tong, Y.; Pang, L. Performance analysis of tower solar aided coal-fired power plant with thermal energy storage. *Appl. Therm. Eng.* **2022**, *206*, 118101. [CrossRef]
18. Jiang, Y.; Duan, L.; Tong, Y.; Yang, M.; Pang, L. Collaborative optimization of thermal and economic performances of a tower solar aided coal-fired power generation system. *Appl. Therm. Eng.* **2022**, *214*, 118885. [CrossRef]
19. Li, B.; Li, Y.; Zhang, Y.; Jia, Y.; Zhang, H.; Chu, X.; Fu, Y.; Yang, T. Simulation study on design and operation characteristics of tower solar-assisted coal-fired power generation system. *Proc. CSEE* **2018**, *38*, 1729–1737.
20. Zhu, Y.; Pei, J.; Cao, C.; Zhai, R.; Yang, Y.; Reyes-Belmonte, M.A.; González-Aguilar, J.; Romero, M. Optimization of solar aided coal-fired power plant layouts using multi-criteria assessment. *Appl. Therm. Eng.* **2018**, *137*, 406–418. [CrossRef]
21. Liu, H.; Zhai, R.; Patchigolla, K.; Turner, P.; Yang, Y. Model predictive control of a combined solar tower and parabolic trough aided coal-fired power plant. *Appl. Therm. Eng.* **2021**, *193*, 116998. [CrossRef]
22. Lei, L.; Liu, X.; Wang, H.; Zou, Y.; Xu, Y.; Xu, M. Performance analysis of a novel mode using solar energy to recycle and reuse water vapor from flue gas of coal-fired power station. *Energy Convers. Manag.* **2023**, *276*, 116537. [CrossRef]
23. Zhang, K.; Liu, M.; Zhao, Y.; Yan, H.; Yan, J. Design and performance evaluation of a new thermal energy storage system integrated within a coal-fired power plant. *J. Energy Storage* **2022**, *50*, 104335. [CrossRef]
24. Zhang, K.; Liu, M.; Zhao, Y.; Zhang, S.; Yan, H.; Yan, J. Thermo-economic optimization of the thermal energy storage system extracting heat from the reheat steam for coal-fired power plants. *Appl. Therm. Eng.* **2022**, *215*, 119008. [CrossRef]
25. Wei, H.; Lu, Y.; Wu, Y.; Li, W.; Zhao, D. Flexible operation system analysis of coal-fired units. *J. Beijing Univ. Technol.* **2022**, *48*, 1307–1318.
26. Wei, H.; Lu, Y.; Liu, J.; Li, W.; Zhao, D. Research on large-scale consumption of renewable energy power generation based on deep peak regulation of coal-fired units based on heat storage. *Therm. Power Gener.* **2023**, *52*, 79–89.
27. Yu, Y.; Wang, Y.; Cao, X. Surficial solar irradiation based on meteorological monitoring combined with ground-based cloud images. *Chin. J. Electron Devices* **2024**, *47*, 134–139.
28. Pu, Z.; Xia, P.; Zhang, L.; Wang, S.; Wang, Y.; Min, M. Comparative analysis of machine learning and statistical methods in solar energy prediction. *Acta Energiae Solaris Sin.* **2023**, *44*, 162–167.
29. Liu, T.; Ye, X.; Cheng, L.; Hu, Y.; Guo, D.; Huang, B.; Li, Y.; Su, J. Intelligent Pressure Monitoring Method of BP Neural Network Optimized by Genetic Algorithm: A Case Study of X Well Area in Yinggehai Basin. *Processes* **2024**, *12*, 2439.
30. Zhu, X.; Yu, Y.; Shi, N.; Xu, L.; Jian, Y. Research on hierarchical optimization of BP Neural Network and its application in wind power prediction. *High Volt. Appar.* **2022**, *58*, 158–163+170.

31. Kim, C.; Kim, H.; Mun, K. Use of the international association for the properties of water and steam (IAPWS) formulations, IAPWS-95 & IAPWS-IF97: Making of Mollier diagram and Ts diagram of water and steam. *Therm. Sci. Eng. Prog.* **2020**, *20*, 100691.
32. Wei, H.; Lu, Y.; Yang, Y.; Zhang, C.; He, C.; Wu, Y.; Li, W.; Zhao, D. Research on influence of steam extraction parameters and operation load on operational flexibility of coal-fired power plant. *Appl. Therm. Eng.* **2021**, *195*, 117226. [CrossRef]
33. Rovira, A.; Montes, M.J.; Valdes, M.; Martínez-Val, J.M. Energy management in solar thermal power plants with double thermal storage system and subdivided solar field. *Appl. Energy* **2011**, *88*, 4055–4066. [CrossRef]
34. Rodríguez, I.; Pérez-Segarra, C.D.; Lehmkuhl, O.; Oliva, A. Modular object-oriented methodology for the resolution of molten salt storage tanks for CSP plants. *Appl. Energy* **2013**, *109*, 402–414. [CrossRef]
35. Xia, Z. Capacity Configuration and Thermal Performance Analysis of Medium-Low Temperature Molten Salt Heat Storage System. Ph.D. Thesis, North China Electric Power University, Beijing, China, 2019.
36. Yu, Q.; Li, X.; Wang, Z.; Zhang, Q. Modeling and dynamic simulation of thermal energy storage system for concentrating solar power plant. *Energy* **2020**, *198*, 117183. [CrossRef]
37. Zaversky, F.; García-Barberena, J.; Sánchez, M.; Astrain, D. Transient molten salt two-tank thermal storage modeling for CSP performance simulations. *Sol. Energy* **2013**, *93*, 294–311. [CrossRef]
38. Xu, H.; Deng, Y. Dependent evidence combination based on shearman coefficient and pearson coefficient. *IEEE Access* **2018**, *6*, 11634–11640. [CrossRef]
39. Zhang, S.; Miao, S.; Yin, B. Economic analysis of multi-type energy storage considering deep peak shaving of thermal power. *Electr. Power Constr.* **2022**, *43*, 132–142.
40. Tao, Y. *Thermal Power Plant*; China Electric Power Press: Beijing, China, 2012; pp. 102–103.

Disclaimer/Publisher's Note: The statements, opinions and data contained in all publications are solely those of the individual author(s) and contributor(s) and not of MDPI and/or the editor(s). MDPI and/or the editor(s) disclaim responsibility for any injury to people or property resulting from any ideas, methods, instructions or products referred to in the content.